The Astronomical Journal, 166:205 (8pp), 2023 November https://doi.org/10.3847/1538-3881/acff5a

GJ 357 d: Potentially Habitable World or Agent of Chaos?

Stephen R. Kane and Tara Fetherolf
Department of Earth and Planetary Sciences, University of California, Riverside, CA 92521, USA; skane@ucr.edu
Received 2023 August 2; revised 2023 September 25; accepted 2023 October 2; published 2023 October 20

Abstract

Multiplanet systems provide important laboratories for exploring dynamical interactions within the range of known exoplanetary system architectures. One such system is GJ 357, consisting of a low-mass host star and three orbiting planets, the outermost (planet d) of which does not transit but lies within the habitable zone (HZ) of the host star. The minimum mass of planet d causes its nature to be unknown, both in terms of whether it is truly terrestrial and if it is a candidate for harboring surface liquid water. Here, we use three sectors of photometry from the Transiting Exoplanet Survey Satellite to show that planets c and d do not transit the host star, and therefore may have masses higher than the derived minimum masses. We present the results for a suite of dynamical simulations that inject an Earth-mass planet within the HZ of the system for three different orbital and mass configurations of planet d. These results show that planet d, rather than being a potentially habitable planet, is likely a source of significant orbital instability for other potential terrestrial planets within the HZ. We find that relatively small eccentricities of planet d cause a majority of the HZ to be unstable for an Earth-mass planet. These results highlight the importance of dynamical stability for systems that are prioritized in the context of planetary habitability.

Unified Astronomy Thesaurus concepts: Exoplanets (498); Exoplanet astronomy (486); Exoplanet dynamics (490); Exoplanet systems (484); Astrobiology (74); Habitable planets (695); Orbital evolution (1178)

1. Introduction

The vast number of exoplanet discoveries have allowed the statistical analysis of planetary systems, inferences of planetary demographics, and their relationship to formation and evolution processes. The orbital and mass distribution within planetary systems has yielded significant insight into the nature of planetary architectures (Ford 2014; Winn & Fabrycky 2015; Mishra et al. 2023a, 2023b) and their relationship to the layout of the solar system (Horner et al. 2020; Kane et al. 2021a). Likewise, the diversity of planetary masses detected has enabled the investigation of the transition between terrestrial bodies and planets with a far more substantial gaseous envelope (Weiss & Marcy 2014; Rogers 2015; Wolfgang et al. 2016; Chen & Kipping 2017; Unterborn et al. 2023). For those planets within the terrestrial regime, the highest priority targets for further study are frequently those that lie within the habitable zone (HZ) of the host star (Kasting et al. 1993; Kane & Gelino 2012a; Kopparapu et al. 2013, 2014; Kane et al. 2016; Hill et al. 2018, 2023). However, presence within the HZ is not a sufficient requirement for planetary habitability as there are a vast number of stellar, planetary, and system properties that can influence the long-term sustaining of surface liquid water. Among these many habitability factors are the eccentricity (Williams & Pollard 2002; Dressing et al. 2010; Kane & Gelino 2012b; Linsenmeier et al. 2015; Kane & Torres 2017) and dynamical stability (Kopparapu & Barnes 2010; Kane 2015; Kane & Blunt 2019; Kane et al. 2022) of planets within the HZ, both of which can play a crucial role in their insolation flux variability, or even orbital viability.

A planetary system of recent interest is the GJ 357 system, with an architecture consisting of an M-dwarf star harboring three known planets with orbital periods of 4, 9, and 56 days. The planetary system was initially detected via photometry from the Transiting Exoplanet Survey Satellite (TESS; Ricker et al. 2015; Guerrero et al. 2021; Kane et al. 2021b) as the innermost planet was observed to transit the host star. The two outer planets in the system were subsequently detected through radial velocity (RV) observations and reported by two separate teams: Jenkins et al. (2019) and Luque et al. (2019). The RV measurements provided a mass for the transiting inner planet and facilitated atmospheric loss models for the planet in combination with X-ray observations of the host star (Modirrousta-Galian et al. 2020). However, no transits had been detected for the outer two planets and so their measured masses of 3.4 $M_{\oplus}$ for the middle planet and 6.1 $M_{\oplus}$ for the outer planet (planet d) were stated as minimum masses (Luque et al. 2019), leaving open the possibility that subsequent TESS data may yet reveal their transits. Planet d was cited as being of particular interest since it lies within the HZ of the host star, and Kaltenegger et al. (2019) discussed in detail the potential climate in the context of planetary habitability and pathways toward observational confirmation. These discussions assumed the RV mass to be the true mass of the planet, that the planet is terrestrial in nature, and that it lies in a circular orbit.

In this paper, we present new data and calculations for the GJ 357 system to assess the effect that planet d has on the HZ. Section 2 provides calculations of the system HZ, and a discussion of the possible terrestrial nature of planet d, the eccentricity of the orbit, and the detectability of other terrestrial planets in the system. We also present new TESS photometry that rules out transits for planets c and d, and discuss the implications for their true masses. In Section 3, we describe our dynamical simulation that assesses the dynamical viability of an Earth-mass planet within the HZ in the presence of planet d for three different configurations of the planet d mass and eccentricity. We also examine individual cases of injected planets that survive the simulation, but are not long-term stable. Section 4 discusses the consequences of these results for long-

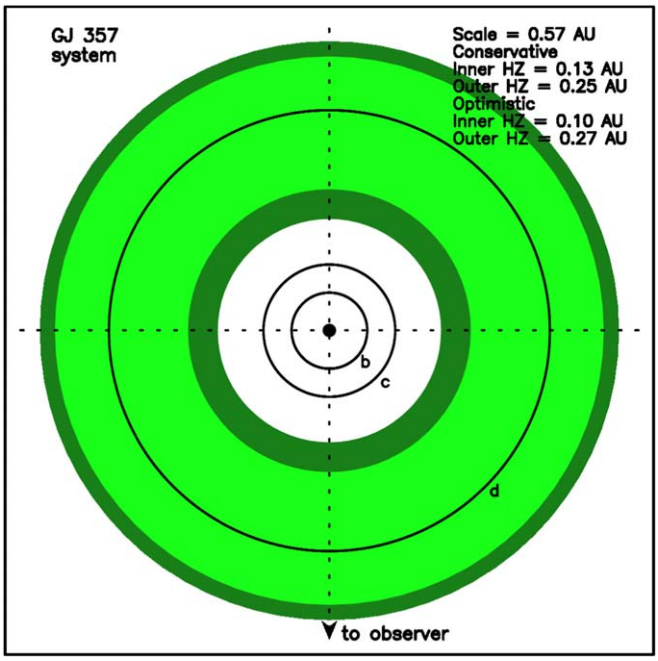

Figure 1. The architecture and HZ of the GJ 357 system, where the scale of the figure is 0.57 au along each side. The CHZ is shown in light green, the OHZ extensions to the HZ are shown in dark green, and the orbits of the known planets are shown as solid circles.

term system stability of possible habitable planets, and the implications for exoplanet demographics within the HZ. We provide suggestions for further work and concluding remarks in Section 5.

2. System Architecture

Here we describe the architecture of the system, calculate the extent of the HZ, and examine TESS data in the context of additional planetary transits.

2.1. Orbits and Habitable Zone

As described in Section 1, the GJ 357 system consists of three known planets orbiting a low-mass star. For the analysis in this work, we adopt the stellar and planetary parameters of Luque et al. (2019). The host star has a spectral classification of M2.5V, with a mass of $M_\star = 0.342\,M_\odot$, a radius of $R_\star = 0.337\,R_\odot$, an effective temperature of $T_{\rm eff} = 3505$ K, and a luminosity of $L_\star = 0.01591\,L_\odot$. These properties allow us to calculate the HZ of the system, including the conservative HZ (CHZ) and the optimistic extension to the HZ (OHZ) based upon the assumption that Venus and Mars had surface liquid water in their past, described in detail by Kane et al. (2016). We calculate distance ranges of 0.131–0.254 au and 0.103–0.268 au for the CHZ and OHZ, respectively. The extent of the HZ and the orbits of the known planets are shown in Figure 1, where the CHZ is shown in light green and the OHZ is shown in dark green, and the semimajor axes of the planetary orbits are 0.35 au, 0.061 au, and 0.204 au for the b, c, and d planets, respectively. It is worth noting that Jenkins et al. (2019) refer to the innermost planets of the system as "c" and "b" in order of increasing semimajor axis, whereas Luque et al. (2019) refer to those same planets as "b" and "c." Here, we adopt the naming convention of Luque et al. (2019), and thus the three planets are referred to as "b," "c," and "d" in order of increasing semimajor axis.

There are various components of the GJ 357 system that remain unconstrained. The planetary orbits shown in Figure 1 are assumed to be circular, and indeed statistical studies have found that smaller planets tend to have relatively low eccentricities (Kane et al. 2012; Van Eylen & Albrecht 2015). Luque et al. (2019) considered eccentric orbits in the preliminary analysis of the RV data, but assumed circular orbits for their final model due to comparable fits between eccentric and noneccentric cases, and the computational burden of including eccentricity as a free parameter. Jenkins et al. (2019) also explored nonzero eccentricities, which included a 1σ eccentricity for planet d consistent with $\sim$0.1, but fixed circular orbits in the final analysis. Thus, an eccentric orbit for planet d is allowable with the present data for the system.

The true architecture of the system is only known to the extent that the sensitivity of the observational data allows, including whether there may be further planets within the system. For example, an additional planet of Earth-mass that lies within the HZ would be challenging to detect with the present data set. We calculate that an Earth-mass planet at the inner and outer edges of the OHZ would have RV semiamplitudes of $0.47\,{\rm m\,s^{-1}}$ and $0.29\,{\rm m\,s^{-1}}$, respectively, which fall below the $2\,{\rm m\,s^{-1}}$ rms precision of the utilized spectrographs. We therefore find that an additional Earth-mass planet in the HZ would likely remain undetectable with the current RV data.

According to Luque et al. (2019), planets c and d have minimum masses of 3.4 and 6.1 Earth masses, respectively. Since planets c and d are not presently known to transit, the true mass of the planets may be significantly higher than the minimum masses. A dynamical analysis of the system performed by Luque et al. (2019) did not place significant constraints on the inclination of planets c and d. However, the dynamical analysis performed by Jenkins et al. (2019), whose RV analysis derived slightly higher planetary masses than those found by Luque et al. (2019), determined that the mass of planet d lies in the range of 7.2–11.2 Earth masses. The resolution on whether or not planet d transits the host star is an important component of understanding the true nature of this HZ planet.

2.2. Planet d does not Transit

The analysis performed by Jenkins et al. (2019) and Luque et al. (2019) used Sector 8 of TESS photometry, which occurred during the TESS Prime Mission. Since then, GJ 357 has been observed again during sectors 35 and 62. The time-series photometry observed by TESS was obtained through the Mikulski Archive for Space Telescopes (MAST Team 2021). We utilize the 2 minutes presearch data conditioning simple aperture photometry (PDCSAP), which was processed by the Science Processing Operations Center pipeline (Jenkins et al. 2016). Figure 2 shows the light curve of GJ 357 for all three TESS sectors, where the transits of GJ 357 b can be plainly seen in the light curve every $\sim$4 days. The transit depth is 1095 ppm, which translates to a radius for planet b of $R_p = 1.217\ R_\oplus$. Given that the average rms scatter for the shown three TESS sectors is 620 ppm, and that planets c and d are more massive than planet b, transits of the outer two planets should be visible in the data if they occur. Indeed, planets of size $1.5\,R_\oplus$ and $2.0\,R_\oplus$ would produce transit depths of

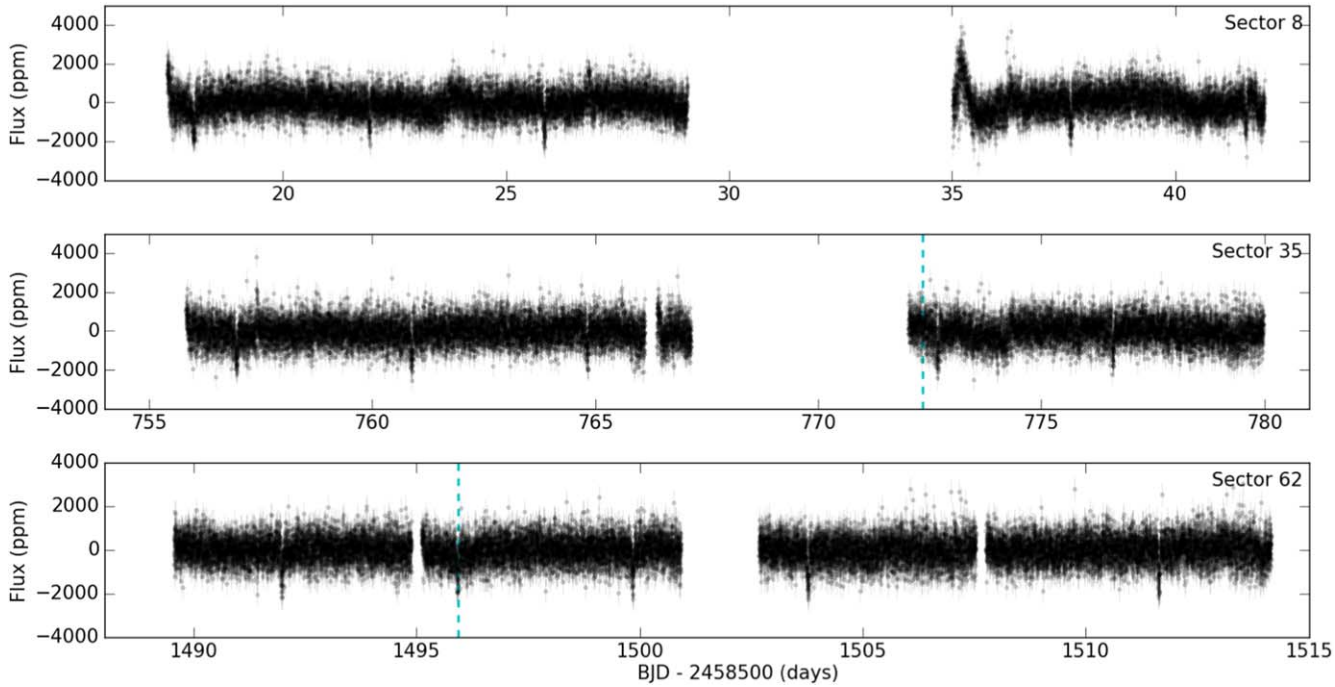

Figure 2. The TESS PDCSAP light curve of GJ 357, which includes photometry obtained during Sectors 8 (top panel), 35 (middle panel), and 62 (bottom panel). Transits of the inner planet, GJ 357 b, can be seen in the light curve every ∼4 days. The vertical dashed lines in the middle and bottom panels indicate the predicted inferior conjunction passage for planet d.

1665 ppm and 2960 ppm, respectively. Assuming the lowest of these radii values, transits of planets c and d are ruled out at 2.7σ per TESS measurement, which is equivalent to that expected for a grazing transit. Based on the system properties described in Section 2.1, we estimate central transit durations of ∼2.0 and ∼3.5 hr for planets c and d, respectively. Thus, central transits for planets c and d are ruled out at a significance of $\sim 21\sigma$ and $\sim 28\sigma$, respectively.

Given the expected transit depths and photometric precision, the three TESS Sectors shown in Figure 2 are sufficient to confirm that planet c (whose orbital period is 9.12 days) does not transit. Planet d has an orbital period of 55.661 days, and so its alignment with a particular TESS sector is less obvious than for planet c. However, the RV orbit shows that an inferior conjunction passage missed Sector 8 entirely, as noted by both Jenkins et al. (2019) and Luque et al. (2019). Using the planet d orbital ephemeris of Luque et al. (2019), we calculate BJD times of inferior conjunction of 2459272.34 and 2459995.93, which occur during the sector 35 and 62 observing windows, respectively. These inferior conjunction times are indicated by the vertical dashed lines shown in Figure 2. The inferior conjunction for sector 35 occurs directly after the telemetry data gap, and reveals no evidence for a transit. The inferior conjunction for sector 62 also falls within the TESS photometry, and in fact falls at the same time as a planet b transit, which would have resulted in a syzygy transit event had planet d transited (Luger et al. 2017; Veras & Breedt 2017). The lack of observable signature at either location verifies that planet d does not transit the host star.

As noted in Section 2.1, the confirmation that planet d does not transit means that the planetary mass may be significantly higher than the minimum mass of $6.1\,M_{\oplus}$. There have been numerous derivations of mass–radius relationships for exoplanets that estimate the upper limits for a terrestrial body (Dressing et al. 2015; Rogers 2015; Chen & Kipping 2017). The empirical relationship between planet mass and radius derived by Chen & Kipping (2017) detected a transition from terrestrial into "Neptunian" planets with a greater volatile inventory at a boundary of $\sim 2\,M_{\oplus}$. Without a radius measurement, there is a great deal of degeneracy regarding the bulk properties of a planet that possibly lies within the terrestrial regime, even if the true mass of the planet is known (Valencia et al. 2007; Dorn et al. 2015; Zeng et al. 2016). The subsolar metallicity of GJ 357 (Luque et al. 2019), combined with the relatively high mass of planet d, suggests the planet lies outside the nominal rocky planet zone (Unterborn et al. 2023). Furthermore, Kopparapu et al. (2014), who assume that planets with masses larger than $5\,M_{\oplus}$ are not rocky, found an increasing rate for the outgoing longwave radiation with planet mass due to the smaller atmospheric column depth, decreasing greenhouse warming and increasing the width of the HZ at the inner edge. With all of these considerations in mind, it is difficult to state with any certainty what the true nature of planet d is, but the minimum planetary mass allows for a large parameter space where a habitable scenario is increasingly unlikely.

3. Dynamical Stability within the Habitable Zone

Here we provide the details and results of an investigation into the dynamical viability of planetary orbits throughout the HZ of the GJ 357 system in the presence of the three known planets.

3.1. Simulation Description

We adopt the methodology described by Kane (2019), Kane et al. (2021c), in which the Mercury Integrator Package (Chambers 1999) was applied with a hybrid symplectic/Bulirsch-Stoer integrator with a Jacobi coordinate system (Wisdom & Holman 1991; Wisdom 2006). Each simulation

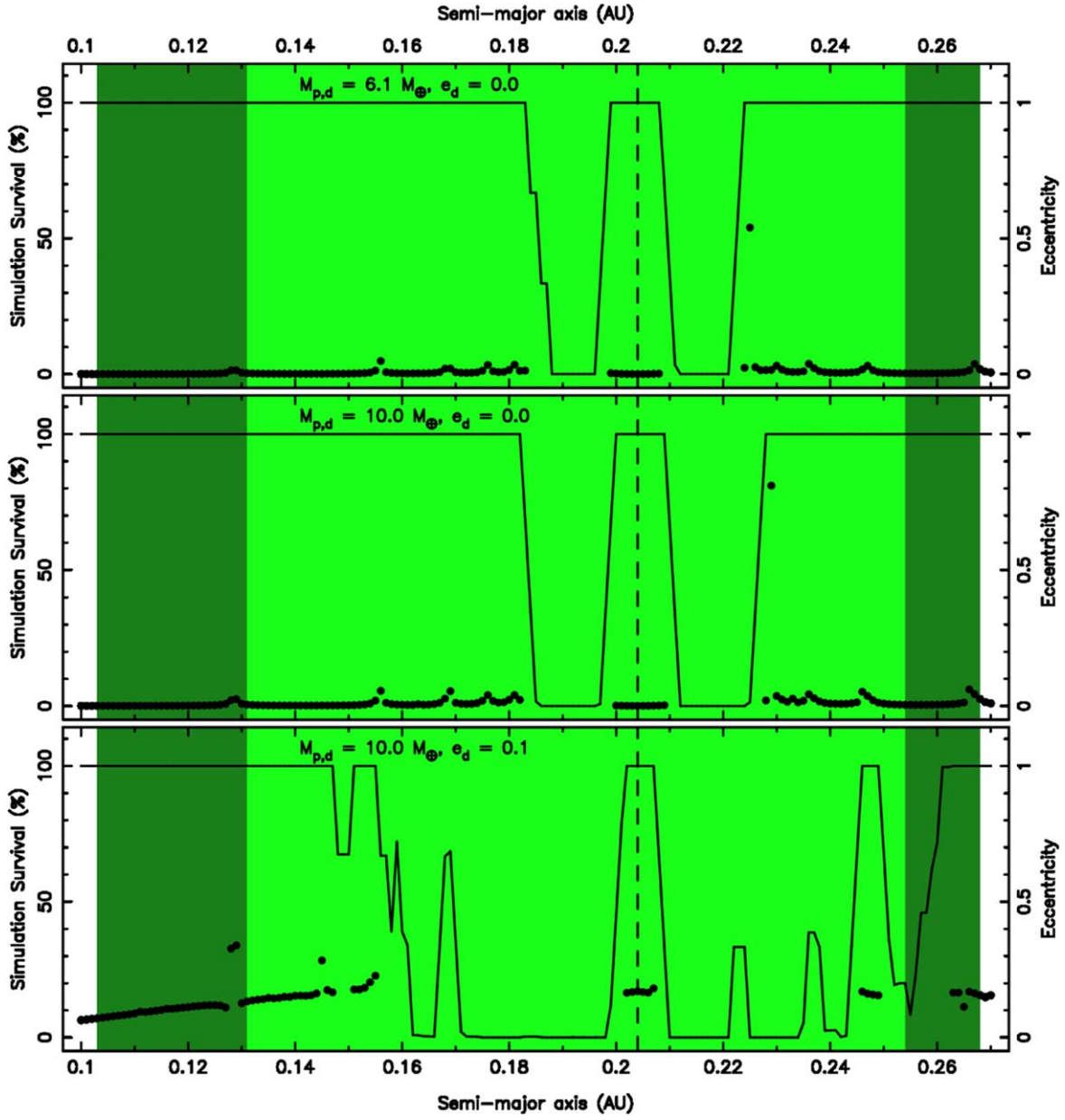

Figure 3. Dynamical stability results for the system architecture cases that vary the inclination, mass, and eccentricity of planet d. Each panel shows the percentage of the simulation that the injected planet survived as a function of semimajor axis, shown as a solid line. As for Figure 1, the CHZ is shown in light green and the OHZ is shown in dark green. The vertical dashed line indicates the semimajor axis of planet d, and the mass and eccentricity for planet d are labeled near the top of each panel. The maximum eccentricities of the injected planet through the simulations are shown as black dots (see Section 3.3).

was integrated for 10^6 yr, equivalent to $\sim 6.5 \times 10^6$ orbits of planet d, and with a time step of 0.1 day to ensure adequate resolution of planet–planet encounters that involve the innermost planet. We used the stellar and planetary properties provided by Luque et al. (2019) and the HZ boundaries calculated in Section 2.1. We tested the orbital stability within the HZ by injecting an Earth-mass planet in a circular orbit that is coplanar with planets b and c, the latter of which is assumed to have a near edge on orbit that allows the minimum planet mass to be adopted as an approximation of the true mass. The new planet was injected at semimajor axes within the range 0.1–0.27 au and in steps of 0.001, encompassing the full OHZ range of 0.103–0.268 au. Additionally, each semimajor axis step incorporated initial evenly spaced mean anomalies of 60°, 180°, and 300° for the injected planet.

Because the orbit of planet d is poorly constrained, our simulations were conducted for three specific orbital configurations of planet d. First, we considered the case of planet d being near coplanar with the other planets such that, like planet c, the minimum planet mass ($6.1\,M_\oplus$) is a reasonable approximation of the true mass. Second, we considered the case of the planet d orbit being significantly inclined with respect to the orbital plane of the other planets, producing a planet mass of $10.0\,M_\oplus$, which is within the dynamical limits found by Jenkins et al. (2019). Third, we considered the case where the orbital inclination and planet mass of planet d is the same as the second case, but now with a slight eccentricity of 0.1. The combination of these three cases resulted in $\sim$1500 simulations in total.

3.2. Simulation Survival Rates

The outcome for each of the simulations described in Section 3.1 was assessed based on the survival of the injected planet, where nonsurvival can mean the planet was either ejected from the system or lost to the gravitational well of the host star. Note that the Mercury Integrator Package assumes point masses, and so planet–planet collisions, though possible, are not considered in the simulations. The results of the simulations are summarized in Figure 3, which contains three panels that represent the results for each of the three orbital configuration cases for planet d mass and eccentricity, shown near the top of each panel. Each panel shows as a solid line the survival time of the injected planet (as a percentage of the full 10^6 yr integration) as a function of the semimajor axis of the injected planet. The HZ is depicted as for Figure 1, with the CHZ shown in light green and the OHZ shown in dark green. The semimajor axis of planet d is indicated by the vertical dashed line. We detected no cases in which any of the three known planets did not survive the simulations, largely due to their substantial mass compared with the injected planet.

For all three cases, there is an island of stability around the semimajor axis of planet d, allowing for the possibility of Trojan planets in similar orbits (Páez & Efthymiopoulos 2015). Remarkably, such Trojan planetary orbits can maintain long-term stability (Cresswell & Nelson 2009; Schwarz et al. 2009), although eccentricity of the primary planet reduces this stable region (Dvorak et al. 2004), as seen in the bottom panel of Figure 3. For the first case ($M_{p,d} = 6.1\ M_\oplus$ and $e_d = 0.0$; top panel), the presence of planet d clears a substantial region around the orbit, and 18% of the HZ is rendered unstable. For the second case ($M_{p,d} = 10.0\ M_\oplus$ and $e_d = 0.0$; middle panel), the instability regions surrounding the orbit of planet d slightly expand to occupy 21% of the HZ. For the third case ($M_{p,d} = 10.0\ M_\oplus$ and $e_d = 0.1$; bottom panel), the introduction of a relatively small eccentricity to the planet d orbit greatly increases the instability with the HZ, resulting in 60% of the HZ being unstable for the injected planet. Instability of the injected planet primarily arises though gravitational perturbations from the known planets, particularly at mea motion resonance (MMR) locations, that increase the eccentricity of the injected planet. Such eccentricity increases are often lead to more frequent perturbations that culminate in the ejection of the planet from the system. These simulation results show that, for the planet mass range explored, increasing the eccentricity of planet d has a larger effect on the instability within the HZ than increasing the planet mass. However, regions of the HZ where the injected planet remains in the system does not guarantee that the planet's orbit is conducive toward potential habitability.

3.3. Eccentricity Consequences

If the injected terrestrial planet in our simulations survived the 10^6 yr integration time, there may remain orbital consequences from interacting with the other planets in the system. In general, compact planetary architectures benefit from stability enabled by the planets' relatively small Hill radii, since that scales linearly with semimajor axis. The results shown in Section 3.2 demonstrate that increasing planet mass, and therefore Hill radius, gradually increases the region of instability surrounding the planet. However, increasing eccentricity has a far greater effect on system dynamics through conservation of angular momentum, and even stable configurations can inherit significant eccentricity evolution cycles.

Another feature shown in Figure 3 is the maximum eccentricity achieved by the injected planet, indicated as black dots in each of the panels. These are shown for the cases where the planet survives the full integration time. The maximum eccentricity values shown for the first two architecture cases (top and middle panels) show that the injected planet eccentricities remain low when the initial conditions of planet d assume a circular orbit. Exceptions to this include slight eccentricity increases at locations of MMR, such as 0.129 au and 0.155 au, corresponding to 2:1 and 3:2 MMR with planet d, respectively. More significant exceptions are those close to the instability regions surrounding planet d, where planetary orbits lie at the edge of chaotic instability. An example of this is shown in Figure 4, which provides the eccentricity evolution for all four planets in the system in the case where $M_{p,d} = 6.1\ M_\oplus$, $e_d = 0.0$, and the injected planet has a semimajor axis of 0.225 au. The data shown in Figure 4 are the first 10^6 yr of an extended 10^7 yr integration conducted to explore the longer-term stability for this particular architecture. The interaction with planet d quickly raises the eccentricity of the injected planet into a quasichaotic state where it remains up until $\sim 0.5 \times 10^6$ yr, even influencing the eccentricity evolution of planets b and c. Beyond $\sim 0.5 \times 10^6$ yr, the injected planet enters into a stable periodic exchange of angular momentum with planet d. Though the injected planet survives the 10^7 yr integration, there is no guarantee that the system will retain stability beyond the simulated period.

The third architecture case (bottom panel of Figure 3) shows a much larger excitation of the injected planet eccentricities, where the maximum eccentricity increases with increasing semimajor axis and remains at ~ 0.2 for the majority of 100% survival simulations. We conducted 10^7 yr simulations for several initial semimajor axis values of the injected planet and found that the planet either did not survive the full simulation or showed increasing signs of chaotic behavior until the end of the simulation. Thus, many of the injected planets in the third architecture case are unlikely to maintain long-term stability beyond the time frame of the simulations shown in Figure 3, particularly at the locations of MMR, due to the chaotic nature of the induced eccentric orbits.

4. Discussion

Jenkins et al. (2019) conducted long-term stability analyses of the GJ 357 system and established that their provided orbital parameters provide a stable configuration. The simulations described in Section 3 were integrated for 10^6 yr and, based on the number of orbits for planet d within that time (see Section 3.1), are generally sufficient to explore the dynamical stability of the presented architecture cases. However, based on the eccentricity evolution results reported in Section 3.3, many of the simulations show evidence for a chaotic divergence from stable configurations beyond the 10^6 time window, which is consistent with the dynamical results for compact multiplanet systems provided by Tamayo et al. (2020). There are numerous circumstances whereby compact multiplanet systems may exhibit the onset of chaotic orbits, most particularly locations of MMR and subsequent secular evolution that modulates MMR widths (Tamayo et al. 2021a, 2021b), such as that seen in Figure 4. Indeed, even the inner planets of the solar system exhibit chaotic behavior over sufficiently long timescales

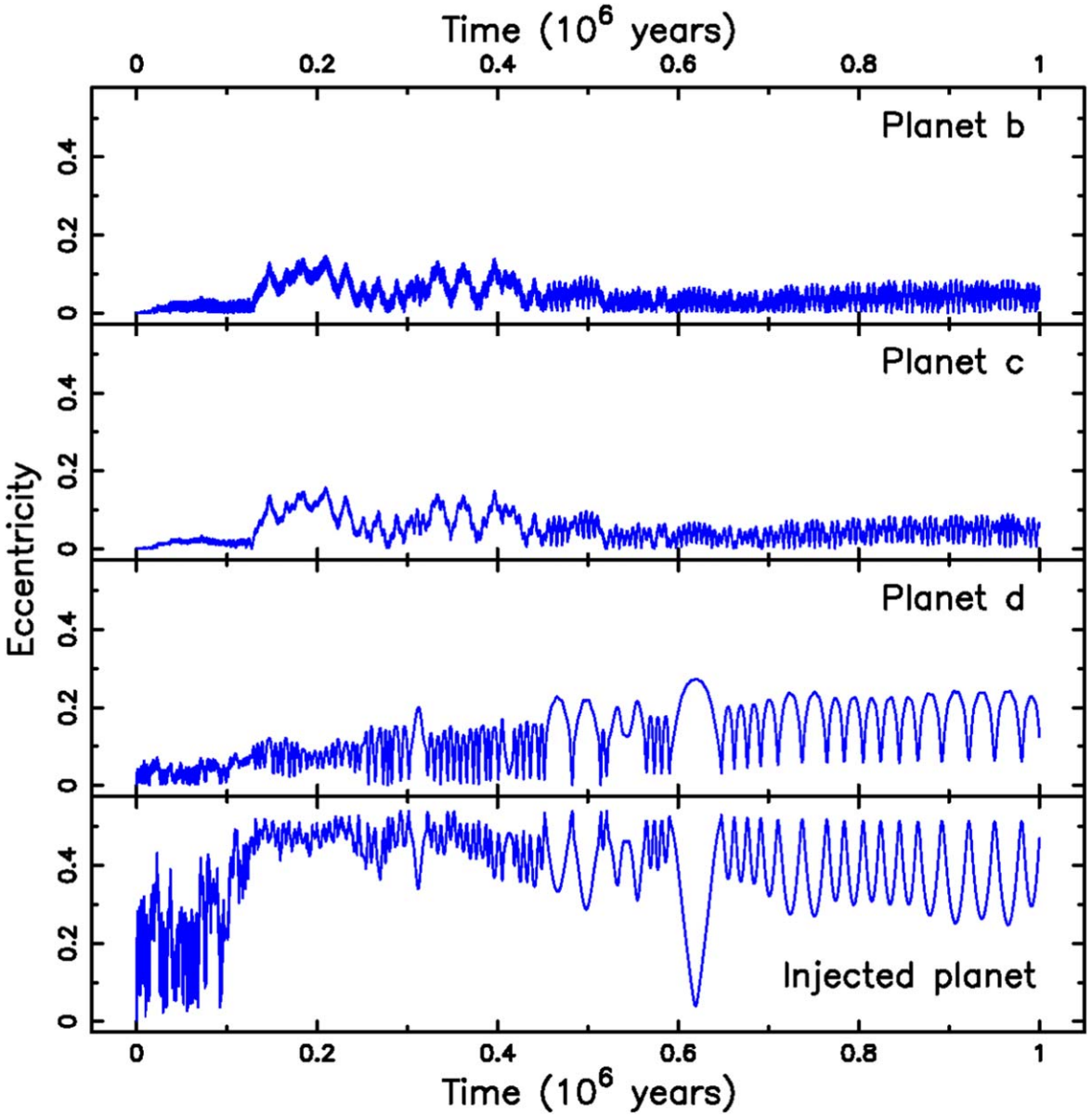

Figure 4. Eccentricity evolution over 10^6 yr for the three known GJ 357 planets and the injected planet for the case of $M_{p,d} = 6.1\ M_\oplus$ and $e_d = 0.0$ and the inserted planet at a semimajor axis of 0.225 au.

(Laskar 1994, 1996). Therefore, the width of the instability regions described in Section 3 and shown in Figure 3 may be considered a lower limit on the induced instability by planet d for each of the three architecture cases.

Terrestrial planets may be optimally packed within the HZ for a wide range of spectral types, provided the orbits are sufficiently circular (Obertas et al. 2017; Kane et al. 2020). As mentioned in Section 1, there has been previous consideration of orbital eccentricity effects on planetary habitability (Williams & Pollard 2002; Dressing et al. 2010; Kane & Gelino 2012b; Linsenmeier et al. 2015; Kane & Torres 2017). Specifically, the orbital modulation of stellar flux received at the top of the atmosphere will influence the planetary climate, depending on the eccentricity and the thermal inertia of the atmosphere that determines the radiative equilibrium timescale (Iro & Deming 2010; Way & Georgakarakos 2017; Kane et al. 2021c). Furthermore, eccentric orbits may induce pseudo-synchronous spins states (Dobrovolskis 2007) and obliquity variations (Deitrick et al. 2018a, 2018b; Vervoort et al. 2022) that impact seasonal modulation of the planetary climate. Planet d will always exchange angular momentum with an injected planet in the HZ, leading to increased eccentricity, often to the point of ejection. Under these conditions, harboring a stable habitable planet within the HZ of GJ 357 system is therefore a challenging scenario.

GJ 357 d may not be a habitable planet, or even terrestrial, and may act to exclude other potentially habitable planets from being present in the system. On the other hand, planet c is almost half the minimum mass of planet d, and is thus more likely to be terrestrial in nature. According to Luque et al. (2019), planet c received a factor of 4.45 more flux from the host star than Earth receives from the Sun. Since planet c lies in the Venus Zone (Kane et al. 2014; Vidaurri et al. 2022), it may be an excellent candidate for a super-Venus, a phrase first coined for the planet Kepler-69 c (Kane et al. 2013). As a nontransiting planet, characterizing the atmosphere of planet c

requires facing the challenge of measuring infrared excess (Stevenson & Space Telescopes Advanced Research Group on the Atmospheres of Transiting Exoplanets 2020), which may be achievable with a space-based mid-infrared low-resolution spectrograph (Mandell et al. 2022). Moreover, GJ 357 b, with a mass of $M_p = 1.84\ M_\oplus$, radius of $R_p = 1.217\ R_\oplus$, and an incident flux of 12.6 times the solar constant (Luque et al. 2019) is another interesting Venus analog candidate that was identified as such by Ostberg et al. (2023). Given the chaotic orbital dynamics resulting from planet d, and the potential for the other known planets to be Venus analogs, the true value of the GJ 357 system may be realized in exploring the boundaries of planetary habitability rather than habitable environments.

5. Conclusions

The GJ 357 system is a fascinating addition to the rapidly growing demographics of compact planetary systems around M-dwarf stars. In the era of TESS, many of these systems are discovered by virtue of the inner planet transiting the host star, and can often lead to ambiguity as to the orbital alignment of other planets detected via the RV technique. Here, we have shown to high statistical significance ($\sim 2.8\sigma$ and $>20\sigma$ for grazing and central transits, respectively) that planets c and d do not transit the host star, raising speculation as to what their true masses may be and if they are terrestrial in nature. Since the overwhelming majority of all planets do not transit from a given vantage point, fully characterizing the bulk of the exoplanet population continues to pose a challenge for exoplanet demographic studies.

GJ 357 d lies within the CHZ of the host star, resulting in the need for understanding the nature of planet d to properly assess the potential for habitable environments within the system. Our dynamical simulations have shown that the most benign architecture scenario, where the true mass of planet d is approximately equivalent to the minimum mass and the orbit is circular, results in 20% of the HZ being unstable for other planets in the system. Even a relatively small eccentricity of 0.1 has the capacity to dramatically increase regions of instability within the HZ, and many of those cases where the injected planet survives our simulations result in chaotic orbits that are unlikely to maintain long-term stability. Therefore, the widths of the instability regions within the HZ are considered lower limits on the potentially chaotic influence of planet d. This means that, though not impossible, it becomes an increasinginly difficult scenario for the system to harbor an additional Earth-mass planet within the HZ as the mass and eccentricity of planet d diverge from their measured lower limits.

Though planet d and its surrounding region may be inhospitable, the GJ 357 system still has much to offer in the study of planetary habitability and evolution. For example, planets b and c may be exceptional candidates for the study of terrestrial planetary evolution in the high-flux regime of M-dwarf stars. Such planets may be analogous to Venus in their evolution, which can retain significant volatiles within a post runaway greenhouse atmosphere (Kane et al. 2019; Way & Del Genio 2020; Krissansen-Totton et al. 2021; Garvin et al. 2022). Thus, the GJ 357 may be an excellent example system to study the boundaries of planetary habitability, refining target selection approaches to narrowing the search for possible habitable worlds.

Acknowledgments

This research has made use of the Habitable Zone Gallery at hzgallery.org. The results reported herein benefited from collaborations and/or information exchange within NASA's Nexus for Exoplanet System Science (NExSS) research coordination network sponsored by NASA's Science Mission Directorate.

Software: Mercury (Chambers 1999).

ORCID iDs

Stephen R. Kane https://orcid.org/0000-0002-7084-0529
Tara Fetherolf https://orcid.org/0000-0002-3551-279X

References

Chambers, J. E. 1999, MNRAS, 304, 793
Chen, J., & Kipping, D. 2017, ApJ, 834, 17
Cresswell, P., & Nelson, R. P. 2009, A&A, 493, 1141
Deitrick, R., Barnes, R., Bitz, C., et al. 2018a, AJ, 155, 266
Deitrick, R., Barnes, R., Quinn, T. R., et al. 2018b, AJ, 155, 60
Dobrovolskis, A. R. 2007, Icar, 192, 1
Dorn, C., Khan, A., Heng, K., et al. 2015, A&A, 577, A83
Dressing, C. D., Charbonneau, D., Dumusque, X., et al. 2015, ApJ, 800, 135
Dressing, C. D., Spiegel, D. S., Scharf, C. A., Menou, K., & Raymond, S. N. 2010, ApJ, 721, 1295
Dvorak, R., Pilat-Lohinger, E., Schwarz, R., & Freistetter, F. 2004, A&A, 426, L37
Ford, E. B. 2014, PNAS, 111, 12616
Garvin, J. B., Getty, S. A., Arney, G. N., et al. 2022, PSJ, 3, 117
Guerrero, N. M., Seager, S., Huang, C. X., et al. 2021, ApJS, 254, 39
Hill, M. L., Bott, K., Dalba, P. A., et al. 2023, AJ, 165, 34
Hill, M. L., Kane, S. R., Seperuelo Duarte, E., et al. 2018, ApJ, 860, 67
Horner, J., Kane, S. R., Marshall, J. P., et al. 2020, PASP, 132, 102001
Iro, N., & Deming, L. D. 2010, ApJ, 712, 218
Jenkins, J. M., Twicken, J. D., McCauliff, S., et al. 2016, Proc. SPIE, 9913, 99133E
Jenkins, J. S., Pozuelos, F. J., Tuomi, M., et al. 2019, MNRAS, 490, 5585
Kaltenegger, L., Madden, J., Lin, Z., et al. 2019, ApJL, 883, L40
Kane, S. R. 2015, ApJL, 814, L9
Kane, S. R. 2019, AJ, 158, 72
Kane, S. R., Arney, G., Crisp, D., et al. 2019, JGRE, 124, 2015
Kane, S. R., Arney, G. N., Byrne, P. K., et al. 2021a, JGRE, 126, e06643
Kane, S. R., Barclay, T., & Gelino, D. M. 2013, ApJL, 770, L20
Kane, S. R., Bean, J. L., Campante, T. L., et al. 2021b, PASP, 133, 014402
Kane, S. R., & Blunt, S. 2019, AJ, 158, 209
Kane, S. R., Ciardi, D. R., Gelino, D. M., & von Braun, K. 2012, MNRAS, 425, 757
Kane, S. R., Foley, B. J., Hill, M. L., et al. 2022, AJ, 163, 20
Kane, S. R., & Gelino, D. M. 2012a, PASP, 124, 323
Kane, S. R., & Gelino, D. M. 2012b, AsBio, 12, 940
Kane, S. R., Hill, M. L., Kasting, J. F., et al. 2016, ApJ, 830, 1
Kane, S. R., Kopparapu, R. K., & Domagal-Goldman, S. D. 2014, ApJL, 794, L5
Kane, S. R., Li, Z., Wolf, E. T., Ostberg, C., & Hill, M. L. 2021c, AJ, 161, 31
Kane, S. R., & Torres, S. M. 2017, AJ, 154, 204
Kane, S. R., Turnbull, M. C., Fulton, B. J., et al. 2020, AJ, 160, 81
Kasting, J. F., Whitmire, D. P., & Reynolds, R. T. 1993, Icar, 101, 108
Kopparapu, R. K., & Barnes, R. 2010, ApJ, 716, 1336
Kopparapu, R. K., Ramirez, R., Kasting, J. F., et al. 2013, ApJ, 765, 131
Kopparapu, R. K., Ramirez, R. M., SchottelKotte, J., et al. 2014, ApJL, 787, L29
Krissansen-Totton, J., Fortney, J. J., & Nimmo, F. 2021, PSJ, 2, 216
Laskar, J. 1994, A&A, 287, L9
Laskar, J. 1996, CeMDA, 64, 115
Linsenmeier, M., Pascale, S., & Lucarini, V. 2015, P&SS, 105, 43
Luger, R., Lustig-Yaeger, J., & Agol, E. 2017, ApJ, 851, 94
Luque, R., Pallé, E., Kossakowski, D., et al. 2019, A&A, 628, A39
Mandell, A. M., Lustig-Yaeger, J., Stevenson, K. B., & Staguhn, J. 2022, AJ, 164, 176
MAST Team 2021, TESS Light Curves—All Sectors, STScI/MAST, doi:10.17909/T9-NMC8-F686
Mishra, L., Alibert, Y., Udry, S., & Mordasini, C. 2023a, A&A, 670, A68

Mishra, L., Alibert, Y., Udry, S., & Mordasini, C. 2023b, A&A, 670, A69
Modirrousta-Galian, D., Stelzer, B., Magaudda, E., et al. 2020, A&A, 641, A113
Obertas, A., Van Laerhoven, C., & Tamayo, D. 2017, Icar, 293, 52
Ostberg, C., Kane, S. R., Li, Z., et al. 2023, AJ, 165, 168
Páez, R. I., & Efthymiopoulos, C. 2015, CeMDA, 121, 139
Ricker, G. R., Winn, J. N., Vanderspek, R., et al. 2015, JATIS, 1, 014003
Rogers, L. A. 2015, ApJ, 801, 41
Schwarz, R., Süli, Á., Dvorak, R., & Pilat-Lohinger, E. 2009, CeMDA, 104, 69
Stevenson, K. B. & Space Telescopes Advanced Research Group on the Atmospheres of Transiting Exoplanets 2020, ApJL, 898, L35
Tamayo, D., Cranmer, M., Hadden, S., et al. 2020, PNAS, 117, 18194
Tamayo, D., Gilbertson, C., & Foreman-Mackey, D. 2021a, MNRAS, 501, 4798
Tamayo, D., Murray, N., Tremaine, S., & Winn, J. 2021b, AJ, 162, 220
Unterborn, C. T., Desch, S. J., Haldemann, J., et al. 2023, ApJ, 944, 42
Valencia, D., Sasselov, D. D., & O'Connell, R. J. 2007, ApJ, 665, 1413
Van Eylen, V., & Albrecht, S. 2015, ApJ, 808, 126
Veras, D., & Breedt, E. 2017, MNRAS, 468, 2672
Vervoort, P., Horner, J., Kane, S. R., Kirtland Turner, S., & Gilmore, J. B. 2022, AJ, 164, 130
Vidaurri, M. R., Bastelberger, S. T., Wolf, E. T., Domagal-Goldman, S., & Kumar Kopparapu, R. 2022, PSJ, 3, 137
Way, M. J., & Del Genio, A. D. 2020, JGRE, 125, e06276
Way, M. J., & Georgakarakos, N. 2017, ApJL, 835, L1
Weiss, L. M., & Marcy, G. W. 2014, ApJL, 783, L6
Williams, D. M., & Pollard, D. 2002, IJAsB, 1, 61
Winn, J. N., & Fabrycky, D. C. 2015, ARA&A, 53, 409
Wisdom, J. 2006, AJ, 131, 2294
Wisdom, J., & Holman, M. 1991, AJ, 102, 1528
Wolfgang, A., Rogers, L. A., & Ford, E. B. 2016, ApJ, 825, 19
Zeng, L., Sasselov, D. D., & Jacobsen, S. B. 2016, ApJ, 819, 127